Food Chemistry 498 (2026) 147187

Contents lists available at ScienceDirect

Food Chemistry

journal homepage: www.elsevier.com/locate/foodchem

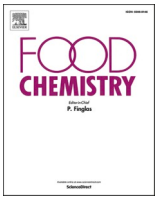

Coconut protein amyloid-like fibrils-based Pickering emulsions of diverse phases: Fabrication, characterization and digestion behavior

Yuanyang Song [a,1], Zhen Yang [a,1], Hui Chen [a], Kaidong Wei [a], Lianzhou Jiang [a,b,c,d], Zhaoxian Huang [a,c,d,*]

[a] School of Food Science and Engineering, Hainan University, Haikou 570228, China
[b] College of Food Science, Northeast Agricultural University, Harbin 150030, China
[c] Collaborative Innovation Center of Nanfan and High-Efficiency Tropical Agriculture, Hainan University, Haikou 570228, China
[d] Hainan International Joint Research Center for High Value Processing of Tropical Protein Resources, Haikou 570228, China

ARTICLE INFO

Keywords:
Coconut protein fibrils
High internal phase Pickering emulsion
In vitro digestion

ABSTRACT

Low, medium, and high-internal-phase Pickering emulsions (PEs) were developed using coconut protein amyloid fibrils (CAF) formed through acid-heat induction. We examined the structural and interfacial properties of CAF and found that they form flexible amyloid fibrils, which facilitate the formation of diverse PEs. PEs with different internal-phases were successfully fabricated using CAF, and their multifunctional performance was characterized through various measurements. PEs with an oil phase volume fraction $\varphi = 0.8$ exhibited larger droplet size and higher zeta-potential, increased viscosity, and enhanced resistance to deformation without defined yield stress point. PEs with $\varphi = 0.2$ demonstrated greater physical stability and improved bioavailability. All PEs showed excellent long-term storage stability (>10 days). Confocal microscopy revealed a blanket-like microstructure and uniform particle distribution. PEs demonstrated high encapsulation efficiency (98.27 %) and a slow digestion rate (1.21 %). This study presents a promising strategy for designing multi-phase PEs stabilized by plant protein-derived amyloid-like fibrils.

1. Introduction

Coconut protein isolate (CPI) is a major biomacromolecule in coconut milk, gaining attention for its high-quality amino acid composition and anti-inflammatory and anti-diabetic properties in recent years (Chen et al., 2024). As a renewable plant-based protein, CPI shows great potential for promoting health and preventing disease, owing to its high arginine content and notable anti-diabetic activity (Chen et al., 2024; Thaiphanit & Anprung, 2016). In addition, coconut protein can act as a natural emulsifier, stabilizing fat globules and forming oil-in-water (O/W) emulsions (Navaf, et al., 2023; Zhu, Chen, et al., 2024). However, natural coconut protein exhibits weaker binding capacity at the oil-water interface than soy, peanut, or quinoa protein (Zhu, Qiu, et al., 2024). The complex protein fractions and structure of raw CPI limit its emulsification, foaming, and antioxidant properties, restricting its broader application (Chen et al., 2024). In recent years, researchers have increasingly explored the high-value use of CPI as an emulsifier, and appropriate modifications have been proposed to further enhance its application potential (Zhu, et al., 2024).

To expand the application of CPI, researchers have investigated a range of modification strategies aimed at improving its structural and functional properties. Traditional modifications, such as physical treatments (e.g., pH, heat, microwave, and high pressure), chemical treatments (e.g., acylation, glycation, and phosphorylation), and enzyme treatments, has been employed as a technology to enhance the application potential of natural proteins (Yang, Song, Chen, Jiang, et al., 2025). However, conventional approaches have shown limited efficiency in improving the structural properties and functional applications of CPI. As a result, the search for novel protein modification technologies has gained increasing attention across diverse fields.

Inspired by co-treatment modification strategies, protein amyloid fibrillation induced by acid-heat treatment has recently attracted growing attention as a promising approach for protein modification and for enhancing techno-functional properties (Liang et al., 2025). Briefly, native protein undergoes misfolding and self-assembles into fibrous aggregates under specific environmental conditions, such as extreme

* Corresponding author at: School of Food Science and Engineering, Hainan University, Haikou 570228, China.
E-mail address: huangzhaoxian@hainanu.edu.cn (Z. Huang).
[1] Co-first authorship, meaning [Yuanyang Song, Zhen Yang] are the co-first authors of this manuscript.

https://doi.org/10.1016/j.foodchem.2025.147187
Received 24 June 2025; Received in revised form 16 October 2025; Accepted 17 November 2025
Available online 24 November 2025

pH, temperature, or ionic concentration. These fibrous aggregates are known as protein amyloid fibrils (AF) (Meng et al., 2022; Xu, Ma, et al., 2023). To date, AF development in the food field has primarily focused on plant proteins such as soybean (Han et al., 2026), pea (Wu et al., 2022), and peanut protein (Meng et al., 2022; Xu et al., 2025a). Compared to animal-based proteins, plant proteins offer greater health benefits, including reduced blood lipid levels and lower risks of diabetes and cancer (Hertzler et al., 2020). Soybean protein-based AF has been used as a Pickering stabilizer to enhance the stability of fat replacers containing red palm oil (Zhou et al., 2025). Li and Wang (2023) used rice glutelin-based AF to construct a Pickering emulsion that enhances bioactive bioaccessibility. Recent studies suggest that AF formation primarily relies on aggregation-prone regions (APRs) in native protein domains, which exhibit high hydrophobicity and a strong propensity to form β-sheets (Liang et al., 2025). Although AF formation varies by source, it generally follows a continuous process of nucleation, growth, and maturation. Compared with other natural plant proteins, CPI could serve as a potential AF-based Pickering stabilizer due to its native characteristics: (I) low solubility or tendency to form insoluble aggregates under neutral conditions, (II) high hydrophobic amino acid content promoting hydrophobic APR formation, and (III) high β-sheet content facilitating structural stacking in AF. These characteristics were supported by the previous findings (Chen et al., 2024; Yang, Song, Chen, Wang, et al., 2025). Thus, we hypothesize that in situ fibrillization of CPI can markedly improve its physicochemical and functional properties, enabling it to act as an effective Pickering stabilizer for the formation of plant protein-based Pickering emulsions.

This study successfully developed a novel flexible AF from CPI, which demonstrated superior wettability and flexibility compared with other plant-based AFs. CAF was then utilized to prepare multiphase Pickering emulsions characterized by highly stable and dense network structures. A combination of analytical methods was applied to investigate the formation mechanism of AFs, characterize the properties of the Pickering emulsions, and evaluate their digestion behavior. These techniques contain particle size analysis and zeta potential evaluation, microstructural observation, infrared and fluorescence spectroscopy, and thermic assessment. This work offers valuable insights into the design of novel plant-based alternative proteins and their application as delivery systems for bioactive substances.

2. Material and methods

2.1. Materials

Fresh coconut milk was purchased from Tai Feng Co., Ltd. (Hainan, China). Medium-chain triglyceride (MCT) oil was obtained from Musim Mas Holdings Pte. Ltd. (Singapore). Simulated gastric fluid (CF-006) and simulated intestinal fluid (CW-005) were both purchased from Chuangfeng Automation Technology Co., Ltd. (Dongguan, China). All other chemical reagents were supplied by Macklin Biochemical Technology Co., Ltd. (Shanghai, China).

2.2. Isolation of CPI from coconut milk

Coconut protein isolate (CPI) was isolated with slight modifications to a previously reported method by our team (Yang, Song, Chen, Zhang, et al., 2025). Briefly, fresh coconut milk was centrifuged at 8000 rpm for 20 min at 4 °C using a high-speed centrifuge. The pH of the supernatant was adjusted to 4.1, and the mixture was incubated at 4 °C for 2 h. The mixture was then centrifuged again under the same conditions. The resulting protein-rich precipitate was collected and washed three times by centrifugation with Milli-Q water. The washed precipitate was dialyzed and then lyophilized for 48 h to obtain CPI. The protein content of CPI was determined to be 92.5 g/100 g using the Kjeldahl nitrogen method (Punzalan et al., 2025).

2.3. Preparation of CAF

The previously obtained CPI was used to prepare coconut protein amyloid fibrils (CAF), following a modified method based on Frey et al. (2024). First, CPI (1.0 g) was dispersed in 100 mL of Milli-Q water and hydrated at 4 °C for 12 h. The pH of the mixture was adjusted to 2.0 and then centrifuged at 10000 ×*g* for 30 min at 4 °C to remove insoluble precipitates. The supernatant was transferred to a water bath and heated at 85 °C for 20 h with constant stirring at 700 rpm. The heated solution was then rapidly cooled in an ice water bath to stop the reaction. The final products were frozen at −80 °C and lyophilized for 48 h.

2.4. Atomic force microscopy (AFM)

AFM images (2.5 × 2.5 μm) of CAF were acquired using a Bruker Dimension Icon (Bruker Corp., Karlsruhe, Germany) at a scan rate of 1.5 Hz. The sample was diluted to 0.01 mg/mL and deposited onto mica flakes. The sample was then dried at 25 °C for 12 h (Frey et al., 2024).

2.5. Determination of CAF structure

2.5.1. X-ray diffraction (XRD)

The crystal structures of CPI and CAF were analyzed using a SmartLab X-ray diffractometer (Rigaku, Japan) equipped with a two-dimensional silicon array detector, following the method described by Yang, Zeng, Chen, Tian, et al. (2025). Samples were mounted on a glass plate and leveled to ensure a smooth surface. Diffraction was recorded over a 2θ range of 4°–50° using Cu Kα radiation (λ = 1.540 Å) at 60 mA and 40 kV. The slit width was set to 0.5 mm, with a scanning rate of 10°/min.

2.5.2. Fourier transform infrared spectroscopy (FTIR)

The FTIR spectra of CPI and CAF were obtained using a T27 FTIR spectrometer (Bruker Corporation, Germany), following the method by Yang et al. (2025). Lyophilized samples were mixed with potassium bromide (KBr) at a ratio of 1:150 and compressed into transparent pellets. Spectra were recorded in the range of 400–4000 cm^{-1} with a resolution of 4 cm^{-1}. Each spectrum was obtained by averaging 64 scans at room temperature. The resulting spectra were analyzed using OMNIC 9.12 software.

2.5.3. Intrinsic fluorescence

Fluorescence spectra of CPI and CAF were recorded using an F-4700 fluorescence spectrometer (HITACHI, Japan), following the method described by Yang et al. (2025). Sample solutions (1.0 mg/mL) were prepared in 0.1 M phosphate buffer (pH 7.0). The emission spectra were recorded from 290 to 500 nm, with an excitation wavelength of 280 nm. The slit width and PMT voltage were set to 5 nm and 700 V, respectively. Measurements were conducted at a scanning speed of 1200 nm/min.

2.6. Determination of surface tension for CAF

Surface tension measurements of CPI and CAF were conducted according to the method described by Yang et al. (2025). Briefly, sample solutions (1.0 mg/mL) were prepared in Milli-Q water and equilibrated for 12 h. A syringe needle was immersed in MCT oil to form a 20 μL droplet. Surface tension was recorded over a period of 10,800 s, with data collected every 10 s. Surface tension (S) was calculated using the following equation:

$$\sigma = \Delta\rho \bullet \frac{g}{C} \tag{1}$$

$$S = \sigma_1 - \sigma_0 \tag{2}$$

where S is the surface tension of sample, $\Delta\rho$ is the density difference between sample solution (1.0048 g/cm^3) and oil phase (0.9398 g/cm^3),

g is the gravitational acceleration, C is the capillary constant, σ_1 and σ_0 is the surface tension of sample solution and buffer solution, respectively.

2.7. Determination of the interface contact angle for CAF

The interfacial contact angles of CPI and CAF were measured following the method reported by Yang et al. (2025). Samples were compressed into sheets of several millimeters in thickness, immersed in MCT for 1 min, and the excess oil on the surface was carefully removed. Measurements were carried out using the sessile drop method with an interfacial tension analyzer (OT100, Ningbo NB Scientific Instruments Co., Ltd., China). Specifically, each sheet was placed on the analyzer stage, and 3 μL of Milli-Q water was carefully dispensed onto its surface. Images were captured after 10 s of equilibration, and contact angles were calculated using the Laplace-Young equation.

2.8. Preparation of CAF-based Pickering emulsions

The preparation of CAF-based Pickering emulsions (PEs) was performed with minor modifications to the method described by He et al. (2024). Briefly, a CAF solution (20 mg/mL) was prepared in Milli-Q water with constant stirring for 30 min. Subsequently, the CAF solution was mixed with MCT oil at volume ratios of 8:2, 1:1, and 2:8, referred to as $PE_{2:8}$, $PE_{1:1}$, and $PE_{8:2}$, respectively. Prior to high-pressure homogenization (30 MPa and 3 cycles), the mixtures were pre-homogenized using a high-speed homogenizer at 5000 rpm for 30 s. The resulting PEs were stored at 4 °C for further analysis. Notably, natural CPI cannot form stable emulsions, so it would not be pursued further in this study.

Curcumin loading into the Pickering emulsion was carried out as follows: Curcumin (1 mg/mL) was dissolved in MCT oil and sonicated in an ultrasonic cleaner (LC-MUC, LIChEN Technology Ltd., China) for 2 h at 30 °C and 600 W. The mixture was subsequently stirred in the dark for 12 h to ensure complete dissolution of curcumin.

2.9. Determination of droplet properties

The average droplet size, polydispersity index (PDI), and zeta potential of CPI, CAF, and CAF-stabilized PEs were measured using dynamic light scattering (DLS) with a Zetasizer Nano ZSE (Malvern Instruments Ltd., UK), following the method described by Zhang et al. (2025). Samples were diluted 20-fold with Milli-Q water prior to measurement. The medium refractive index and sample refractive index were set to 1.330 and 1.460, respectively. Measurements were performed at room temperature in triplicate.

2.10. Determination of rheological properties

The rheological properties of CAF-stabilized PEs were assessed using a Discovery HR rheometer (TA Instruments, USA) with a parallel-plate geometry (1 mm gap) at 25 °C, following the method described by Yang et al. (2025). Emulsion samples (1 mL) were placed at the center of the rheometer plate, and rheological measurements were performed within the linear viscoelastic region. The measurement parameters were set as follows:

2.10.1. Apparent viscosity

The apparent viscosity of the samples was measured over a shear rate range of 1–100 s^{-1} using a dynamic continuous shear scan mode, with a total shear time of 600 s. The relationship between apparent viscosity and shear rate was modeled using the power-law equation:

$$\eta = K\,\gamma^{n-1} \tag{3}$$

where η is the apparent viscosity (Pa·s), γ is the shear rate (s^{-1}), K is the consistency coefficient (Pa·s^n), and n is the flow behavior index.

2.10.2. Frequency sweep

The rheological properties of the PEs within the linear viscoelastic region (LVR) were measured using a frequency sweep from 0.1 to 100 Hz with a parallel plate geometry (PP50). A constant shear strain of 0.01 % was applied throughout the measurement.

2.11. Microstructural observation

To investigate the microstructure of CAF and PEs, optical images were captured using an optical microscope (BK-POL, Optec, China) equipped with a polarized light system, while confocal laser scanning microscopy (CLSM) images were obtained using a Nikon CLSM (A1RHD25, Japan) (Yang, Song, Chen, Jiang, et al., 2025). For optical microscopy, a CAF solution (1 mg/mL) was prepared in Milli-Q water. A 10 μL droplet was placed on a glass slide and observed under 10× and 100× magnifications. For CLSM imaging, 1 mL of PE was mixed with 100 μL of a fluorescent dye mixture containing Nile Blue (0.1 wt%, *w/v*) and Nile Red (0.1 wt%, w/v). The excitation wavelengths were set at 488 nm and 633 nm, respectively.

2.12. Determination of long-term and physical stability

The long-term physical stability of CAF-stabilized PEs was assessed by visual observation and using a physical analyzer (LUMisizer-651, Germany), following the method described by Yang et al. (2025). Samples were loaded into centrifuge tubes, and data were collected at a centrifugal speed of 4000 rpm with a wavelength of 870 nm.

2.13. Encapsulation of curcumin

To explore the potential applications of CAF-stabilized PEs, curcumin was encapsulated within the emulsion. The encapsulation efficiency (EE) of the bioactive compound was determined following the method previously described by Yang et al. (2025). Briefly, curcumin-loaded PEs were mixed with ethanol at a 1:10 (*v/v*) ratio using a vortex mixer. The mixture was then centrifuged at 4500 rpm for 5 min to collect the supernatant. Curcumin concentration in the supernatant was quantified using a UV spectrophotometer at 426 nm. EE was calculated using the following equation:

$$EE = \frac{m_1}{m_2} \times 100 \tag{3}$$

Where m_1 is the encapsulated content of curcumin and m_2 is the total content of curcumin.

2.14. In vitro digestion evaluation

The in vitro digestive properties of CAF-stabilized PEs in the gastrointestinal tract were evaluated with slight modifications based on the method described by Kuzhithariel Remanan and Zhu (2023). Briefly, the emulsion droplets were mixed with simulated gastric fluid (2 g/L NaCl,7 mL/L HCl, and 3.2 g/L pepsin) at a 1:1 mass ratio, and the pH of the mixture was adjusted to 2.0. The mixture was shaken at 37 °C for 1 h, then mixed with simulated intestinal fluid (8.34 g/L $CaCl_2$, 43.74 g/L NaCl, 25.2 g/L bile salt solution, 8.4 g/L pancreatic enzyme solution, and 8.4 g/L lipase solution) at a 1:1 ratio. The pH of the resulting mixture was adjusted and maintained at 7.0 using 0.1 M NaOH. After digestion, the digestive fluid was centrifuged at 4 °C and 10,000 rpm for 30 min. The resulting permeable mixed micellar phase was collected, mixed with anhydrous ethanol, and centrifuged at 3000 rpm for 10 min. The absorbance of the supernatant at 425 nm was measured, and the curcumin concentration was determined using a standard curve prepared in anhydrous ethanol. Curcumin bioaccessibility was calculated as the ratio of curcumin content in the mixed micellar phase to that in the digestive fluid. The released free fatty acid (FFA) content was calculated using the following equation:

$$FFA(\%) = \frac{C_1 \times V_1 \times m_1}{m_2} \times 100 \quad (4)$$

where C_1 is the concentration of the NaOH solution, V_1 is the consumed volume of NaOH (0.1 mol/L), m_1 is the molecular weight of lipid (242.34), and m_2 is the lipid weight in the system.

2.15. Statistical analysis

All measurements were performed in triplicate or more. Experimental results are presented as mean ± standard deviation. Statistical analysis was performed using one-way ANOVA in SPSS version 17.0 (SPSS Inc., Chicago, IL), with a significance level set at 95 % confidence ($p < 0.05$).

3. Results and discussions

3.1. Structure and interfacial properties of CAF

3.1.1. Formation of CAF

Generally, amyloid fibrils form through extensive aggregation and self-assembly of unfolded protein molecules. Under microscopic observation, amyloid fibrils typically appear as chain-like structures, in which β-sheet protein subunits twist along the fibrils and stack through aggregation (Meng et al., 2022; Xu, Zhou, et al., 2023). Therefore, to investigate CAF formation in this study, its morphology and structure are shown in Fig. 1. As shown in Fig. 1A and B, CPI presented a typical layered structure composed of spherical aggregates, CAF appeared as flexible fibrils without branched chains under polarized light microscopy. This observation aligns with previous reports (Fu et al., 2023; Liu et al., 2025). Moreover, fibrils extended up to several tens of micrometers in length, indicating higher fibrillization of CAF compared to previous studies that reported broader length distributions (vanden Akker et al., 2011). The formation of long fibrils facilitates their role as interfacial particles in Pickering emulsions, primarily due to altered wettability at the oil-water interface (Xu et al., 2025b).

3.1.2. Structure characterization of CAF

To elucidate the structural characteristics of CPI and CAF, infrared spectroscopy and secondary structure analyses were first performed. To ensure accuracy, the fibril solution was dialyzed (10–12 kDa cutoff membrane) to remove excess non-fibrillar proteins and other impurities prior to structural characterization. As shown in Fig. 1C, The C—H vibrational peak of CPI exhibited a pronounced blue shift (2939.6 to 2960.5 cm^{-1}) and reduced peak intensity following fibrillation, indicating that CAF formation accompanied by hydrophobic interactions and hydrogen bonding, thereby enhancing the surface wettability of CAF (Zhao, Liang, et al., 2024). The peak at 1650 cm^{-1} arises from the stretching vibrations of C—N and C═O in the amide I band, which closely relates to the main chain conformation (Wang et al., 2025). Compared to CPI, the amide I peak shifts from 1650 cm^{-1} to 1647 cm^{-1}, a typical blue shift indicating structural reorganization. This shift reflects the formation of intermolecular β-sheet structures in fibrils, distinct from the intramolecular β-sheets in the native protein. A similar observation was also reported in previous studies (Wang et al., 2025). The absorption peak at 1236 cm^{-1} in the amide III region corresponds to N—H bending and C—H stretching vibrations, attributable to the presence of β-sheet structures. For CAF, the spectrum exhibits a pronounced enhancement at this peak, further confirming the increased β-sheet content (Zhao, Wu, et al., 2024). Furthermore, the secondary structure composition of CPI and CAF was analyzed using Gaussian peak fitting, as shown in **Fig. S1**. The results show a decrease in ordered helical structures after fibrillation, accompanied by an increase in folded and amorphous regions. This is attributed to the formation of a spatial zipper structure during the fibrillation process, which grows as the protein undergoes cleavage, thereby generating CAF with high aspect ratios and flexibility (Eisenberg & Sawaya, 2017). Compared to previous studies that mainly focus on hydrogen-bonded core structures, it is notable that amorphous regions may form on the fiber surface. These regions represent another form of protein disorder and misfolding, likely driven by hydrophobic interactions. Amorphous aggregates arise from partially folded intermediates driven by hydrophobic forces. These aggregates typically lack ordered secondary structures, showing a reduction in alpha helices (18.51 % to 3.3 %) and transforming into amorphous regions (18.54 % to 28.07 %). Amorphous regions predominantly localize in the lateral sequences outside the amyloid fiber core, forming a relatively flexible outer layer that enhances interfacial flexibility (Xu et al., 2023). Currently, most research on amyloid fiber structure focuses on the fiber core, with relatively little attention paid to the lateral regions.

To further elucidate the formation of CAF, the XRD patterns of CPI and CAF are presented in Fig. 1D. Serving as a hallmark of amyloid fibrils, the XRD results confirm the presence of the characteristic cross-β structure. As shown in Fig. 1D, two distinct peaks appear at 8.5° and 18.8°, corresponding to d-spacings of 10.3 Å and 4.7 Å, respectively. These peaks are commonly recognized as signature reflections of the amyloid fibrillary cross-β sheet structure (Xu et al., 2025b). Notably, the diffraction peak intensities of CAF decrease compared to CPI, which can be attributed to an increased amorphous region, consistent with the secondary structure analysis shown in **Fig. S1**. The presence of these amorphous regions likely contributes to enhanced wettability at the oil–water interface.

Intrinsic fluorescence spectra can reveal structural and conformational changes in biomacromolecules by monitoring aromatic amino acids such as tryptophan (Trp) and tyrosine (Tyr). Changes in the tertiary environment around aromatic residues are reflected in the fluorescence signals. The intrinsic fluorescence spectra of CPI and CAF are presented in Fig. 1E. As shown, compared to untreated CPI, CAF exhibits a pronounced red shift in emission wavelength. This shift likely results from the shielding of aromatic residues due to protein rearrangement and acid hydrolysis occurring during acid-induced fibril formation (Pang et al., 2025). This observation further suggests that increased amorphous fibril regions mask aromatic residues, consistent with prior findings. Similar results have been reported previously (Liu et al., 2025). In summary, these results indicate that the CPI structure undergoes complete unfolding under acid-heat treatment. The exposed hydrophobic regions, β-sheet prone regions, and unfolded protein monomers assemble into flexible CAF via hydrophobic interactions and hydrogen bonding.

3.1.3. Interfacial characterization of CAF

To further elucidate the interfacial properties of CPI and CAF, the surface tension of the samples was measured, as shown in Fig. 1F. For all samples, surface tension gradually decreased with increasing adsorption time. Compared to native CPI, CAF exhibited a lower surface tension, which can be attributed to its greater molecular flexibility and higher surface hydrophobicity. Similar observations have been reported previously (Yue et al., 2022). Notably, during fibril formation, proteins undergo denaturation, which exposes their highly hydrophobic cores. These exposed hydrophobic regions drive protein molecules to self-assemble via hydrophobic interactions, forming protofibrils that subsequently coil into mature fibrils. Consequently, CAF exhibits a reduced α-helix content and an increased β-sheet content (**Fig. S1**). The rigid β-sheet structures of CAF create a more stable gas–liquid interface with reduced interfacial energy. These results indicate that the enhanced interfacial adsorption capacity of CAF contributes to the formation of more stable Pickering emulsions compared to the raw protein, likely due to the development of a more compact interfacial film structure (Yue et al., 2022). Moreover, the flexible protein amyloid can interact with other interfacial components at the oil–water interface, enabling a freer arrangement on the surface of oil droplets (Isa et al., 2011). The observed lower surface tension further reflects the higher adsorption rate of CAF at the interface.

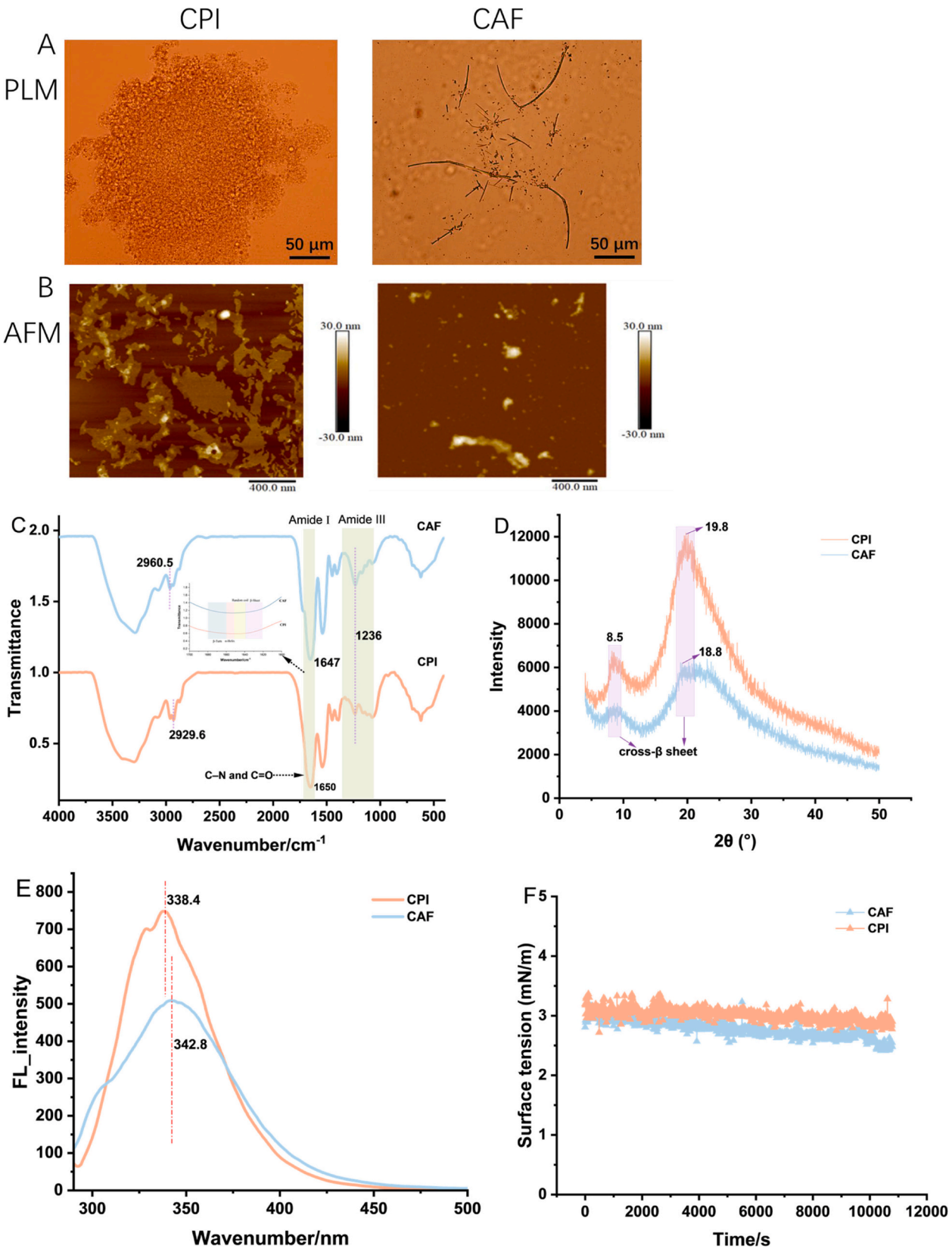

Fig. 1. Microscopic image, structural and interfacial analysis of CPI and CAF. PLM image (A), AFM image (B), FTIR (C), XRD (D), fluorescence spectra (E), and surface tension (F). The scale bar in the microscopic images is 50 μm and 400 nm, respectively. Distinct peaks appear at 8.5°, 18.8° and 19.8°, corresponding to d-spacings of 10.3 Å, 4.7 Å and 4.5 Å, respectively.

The three-phase contact angle further illustrates the relationship between the interfacial behavior and the structure of CAF, as shown in **Fig. S2**. The contact angle of CAF (38.2°) was significantly lower than that of CPI (69.4°), showing a positive correlation with the interfacial tension results (Fig. 1F). This reduction in contact angle is attributed to the adsorption of hydrophilic amino acid residues from CPI onto the surfaces of fibrillar nuclei during fibrillation, promoting the reorganization and assembly into amyloid fibrils enriched in β-sheet structures (Li, Liu, et al., 2025; Meng et al., 2022). In a study on chickpea amyloid fibers, Xiao et al. (2025) demonstrated that during fibrillation, exposed hydrophobic groups on protein surfaces enhance hydrophobic interactions, leading to the formation of fibrillar nuclei. Acidic heat treatment induces the formation of new carboxyl groups in the protein, which further assemble into fibrils, yielding structures with enhanced hydrophilicity (Meng et al., 2022; Xiao et al., 2025). Therefore, these exposed hydrophilic regions endow CAF with enhanced hydrophilicity. Furthermore, compared to CPI, CAF exhibits lower interfacial tension and contact angles, indicating improved droplet spreading and enhanced interfacial wettability (Dev et al., 2025; Restolho et al., 2009). Compared to soy, pea, and chickpea proteins (Han et al., 2026; Li et al., 2023; Xiao et al., 2025), CAF, featuring a hydrophobic core and hydrophilic surface, can rapidly adsorb at the oil–water interface and self-assemble into a network structure. These characteristics effectively prevent oil droplet aggregation, thereby enhancing emulsion stability (Li, Liu, et al., 2025).

3.1.4. Pearson correlation analysis

The Pearson correlation analysis between the interfacial characteristics and structural features of CAF is presented in **Fig. S3**. A high positive or negative correlation coefficient (r) indicates a greater extent of fibrillation and a stronger relationship. An r value between 0.8 and 1.0 is considered indicative of a very strong correlation (Papageorgiou, 2022). FTIR analysis revealed a strong positive correlation with β-sheets, β-turns, disordered regions, hydrophobic domains, and ζ-potential, which are hallmark features of amyloid fiber formation (Xu, et al., 2023). During fibrillation, proteins transition from their native compact globular structures to unfolded states and subsequently reassemble into fibrous structures enriched with cross-linked β-sheets. Exposed hydrophobic regions interact and aggregate, forming ordered fibrous cores connected by disordered flexible chains. Charged amino acid residues, such as lysine and glutamic acid, migrate to the fiber surface and reorganize, thereby forming stable and flexible CAFs (Li et al., 2023; Xu, et al., 2023). Specifically, interfacial tension and contact angles exhibit a strong negative correlation with structural alterations and ζ-potential. This phenomenon may be attributed to nucleation-dependent fibrillation, resulting in rigid core regions of the fibrils and flexible, hydrophilic flanking regions (Xu, et al., 2023). Compared to CPI, CAF exhibits increased surface net charge, reduced interfacial tension, and lower contact angles, indicating improved diffusion properties and enhanced interfacial wettability (Dev et al., 2025). Furthermore, the interfacial properties of CAF are strongly correlated with its structure, necessitating careful control of processing conditions, including ionic strength, pH, protein concentration, and oil content, during emulsification applications.

3.2. Fabrication and characterization of CAF-based PEs

3.2.1. Droplet properties

CAF can function as a Pickering particle, adsorbing at the oil-water interface to establish a robust physical barrier that inhibits droplet coalescence, thus enhancing emulsion stability. To investigate the interfacial behavior of CAF at the oil-water interface, Pickering emulsions (PEs) with different internal phase ratios were prepared and characterized, as shown in Fig. 2. Significant differences were observed in droplet size and zeta-potential among all samples. The droplet size of PEs increased with higher oil content (Fig. 2A). The largest droplet size was observed in $PE_{8:2}$, likely due to insufficient interfacial CAF to fully cover the droplets at high oil ratios. A similar phenomenon was reported previously (Fahim et al., 2025), where droplet size increased with higher oil content in Pickering emulsions. This trend is attributed to the mismatch between droplet volume and increased internal phase, where interfacial particles fail to fully cover all droplets. At a constant CAF concentration, lower oil phase content allows more CAF particles to stabilize droplets, leading to smaller droplet sizes and higher droplet numbers (Fahim et al., 2025). Concurrently, the increase in droplet size can also be explained by the rising viscosity of the system (Winuprasith & Suphantharika, 2015). Maintaining the same droplet size at low oil concentrations requires overcoming a higher interfacial energy barrier. A detailed discussion of system viscosity is provided in the following rheology section. Notably, the polydispersity index (PDI) increased concurrently with droplet size, further confirming the impact of interfacial particles on internal phase formation.

Fig. 2B shows high positive zeta-potential values for all emulsions, indicating strong electrostatic repulsion between droplets and thus good sample stability. The highest (35.6 mV) and lowest (31.2 mV) zeta-potential values were observed in $PE_{8:2}$ and $PE_{2:8}$, respectively, both above 30 mV. Such values suggest a stable emulsion system, where electrostatic repulsion prevents droplet aggregation and flocculation (Fahim et al., 2025). The observed increase in ζ-potential with higher oil content is likely attributable to enhanced adsorption of CAF onto oil droplet surfaces. This effect arises because increasing the oil content expands the total interfacial area that must be stabilized within the emulsion system. Consequently, the concentration of free proteins in the aqueous phase becomes relatively diluted (Tran et al., 2021). To achieve adsorption equilibrium, protein molecules adsorb more strongly and densely at the interface, increasing interfacial adsorption density and

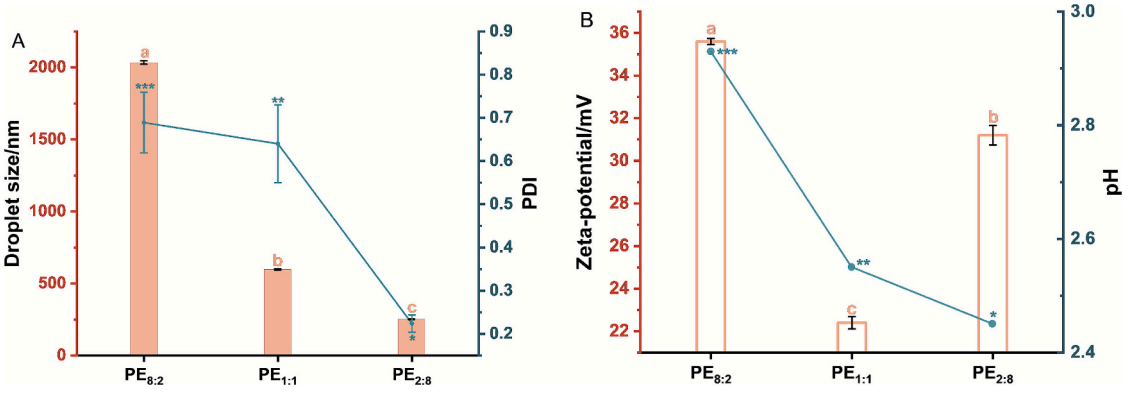

Fig. 2. Droplet properties of CAF-based PEs: droplet size and PDI (A), zeta-potential and system pH (B). Based on variations in the oil-to-water phase ratio, CAF-based emulsions were designated as $PE_{8:2}$, $PE_{1:1}$, and $PE_{2:8}$, respectively. $^{a\text{-}c,\ A\text{-}C}$ Different letters show significant differences between the samples ($P < 0.05$).

consequently elevating the ζ-potential (Sakuno et al., 2008; Tran et al., 2021). Similar results were reported for whey isolate protein amyloid systems (Zhu et al., 2024). Generally, the strength of electrostatic interactions depends closely on the pH of the particle environment. Fig. 2B shows that all samples have low pH values, below the isoelectric point (4.0–4.5) of coconut protein (Yang, Zeng, et al., 2025). This acidic condition promotes stronger interactions with negatively charged molecules.

3.2.2. Rheological properties

Flow behavior.

Fig. 3A shows the apparent viscosity of Pickering emulsions (PEs) with different oil contents stabilized by CAF. All samples exhibited clear shear-thinning behavior, characterized by decreasing viscosity with increasing shear rate. This behavior is typically attributed to the disruption of the emulsion network or droplet deflocculation caused by increased friction from higher shear rates (Boostani et al., 2022). Higher friction facilitates this process within the emulsion system, resulting in a greater apparent viscosity, as observed in $PE_{8:2}$. During shear treatment, large clusters in the emulsions broke down into smaller clusters as shear force increased. A similar phenomenon was reported in a previous study (Yang et al., 2025). Furthermore, the increase in droplet size discussed in section 3.2.1 affects the overall emulsion viscosity, as reflected in this section. The formation of larger oil droplets reduces the spacing between droplets, which increases friction and enhances the modulus of the entire emulsion system.

Small amplitude oscillatory shear (SAOS).

Fig. 3B presents the frequency sweep results of Pickering emulsions (PEs) with varying oil contents stabilized by CAF, showing storage modulus (G') and loss modulus (G") over the range of 1–100 Hz. In all samples, G' remained consistently higher than G" across the entire frequency range, indicating that the elastic response dominates the rheological behavior of the PEs. This resistance to external deformation is attributed to the coating of CAF on the droplet surfaces. The observed elasticity likely arises from non-covalent interactions involving surface groups of the restructured CAF. Additionally, both moduli exhibited slight dependence on frequency within the 0.1–10 Hz range, reflecting the excellent deformation resistance and stability of the CAF-stabilized PEs. Notably, PEs with 0.8 volume fraction (φ) showed higher G' values, which can be explained by stronger droplet interactions and increased system viscosity due to more closely packed oil droplets. These findings suggest that CAF-stabilized PEs possess superior processability, beneficial for applications in emulsion formulation.

3.2.3. Microstructural observation

Optical microscopy and CLSM were employed to characterize the microstructure of PEs stabilized by CAF at oil phase ratios (φ) of 0.2, 0.5, and 0.8. As shown in Fig. 4, the emulsions exhibited a heterogeneous droplet distribution and an internal crosslinked network formed by CAF surrounding the droplets, which varied with oil content. Optical microscopy confirmed the presence of a gel-like internal network in all PEs. With increasing oil content, the network density increased, reflecting the formation of more tightly packed droplets. Furthermore, polarized light microscopy revealed that CAF formed a complex coating around the droplets in all samples, indicating its effective role in stabilizing PEs across different oil phase ratios.

To further clarify the mechanism by which CAF stabilizes the oil-water interface and facilitates PE formation, CLSM images were obtained and are presented in Fig. 4B. A distinct emulsion network was observed in the PEs, characterized by dense cross-linking primarily composed of CAF (green phase), which stabilizes the emulsion system. The oil droplets (red phase) were uniformly dispersed within this "blanket-like" cross-linked network. This typical network structure differs from previous studies focusing on peanut protein isolate amyloid-like fibers stabilizing PEs (Zhao, Liang, et al., 2024). Generally, protein-based Pickering particles uniformly adsorb onto oil droplet surfaces in emulsions (Zhao, et al., 2024). The CLSM results thus confirm the successful formation of CAF-stabilized PEs. Moreover, the denser crosslinked network provides robust structural support, consistent with the rheological behavior described earlier. The network density varied with the internal phase ratios. This interconnected network acts as a three-dimensional barrier that prevents oil droplet aggregation, and this steric hindrance enhances the stability of PEs.

3.2.4. Long-term and physical stability

Fig. 5A shows visualization images of PEs with varying internal phase ratios during storage. No significant changes were observed in the emulsions after 10 days, indicating that CAF-stabilized PEs maintained stability without phase aggregation or separation. This superior stability is attributed to several factors, including the formation of a denser cross-linked network and strong electrostatic repulsion between droplets. Similar findings were reported in a previous study investigating the effects of various glycated globulins on stabilizing high internal phase Pickering emulsions (Yang, Song, Chen, Jiang, et al., 2025).

To further assess the stability of PEs stabilized by CAF, physical stability was evaluated by monitoring transmission changes using a LUMisizer. The transmission curves and integral transmission ratios are presented in Fig. 5B. In the images, the red curve at the bottom and the green curve at the top represent the start and end of the experiment, respectively. An increase in the area under the transmittance curve during centrifugal processing indicates reduced PE stability. As shown in Fig. 5B, compared to $PE_{1:1}$, both $PE_{2:8}$ and $PE_{8:2}$ exhibited higher physical stability, evidenced by a larger proportion of the region with transmission close to zero. This can be attributed to a denser structural network at high internal phase ratios and enhanced interfacial coverage by Pickering particles at low internal phase ratios. These findings align with previous results, and similar phenomena were reported in another study (Zhou et al., 2025). In summary, PEs stabilized by CAF at oil fractions of 0.2, 0.5, and 0.8 retained solid-like properties after 10 days of storage, highlighting their promising potential for applications in bioactive delivery.

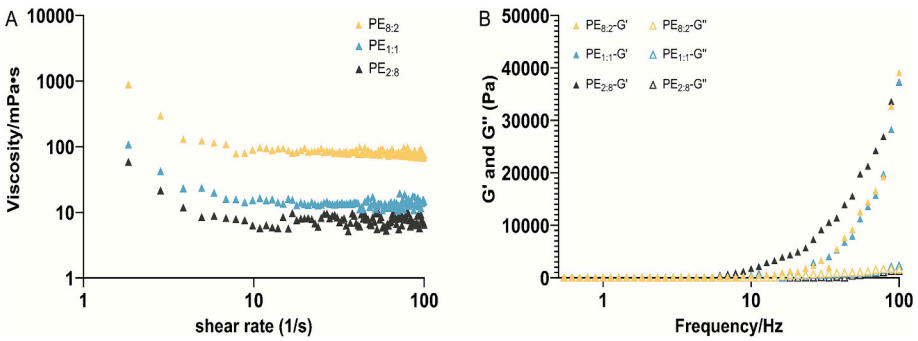

Fig. 3. Rheological properties of CAF-based PEs ($PE_{8:2}$, $PE_{1:1}$, and $PE_{2:8}$) were measured at 25 °C: apparent viscosity versus shear rate (A) and frequency sweeps (B).

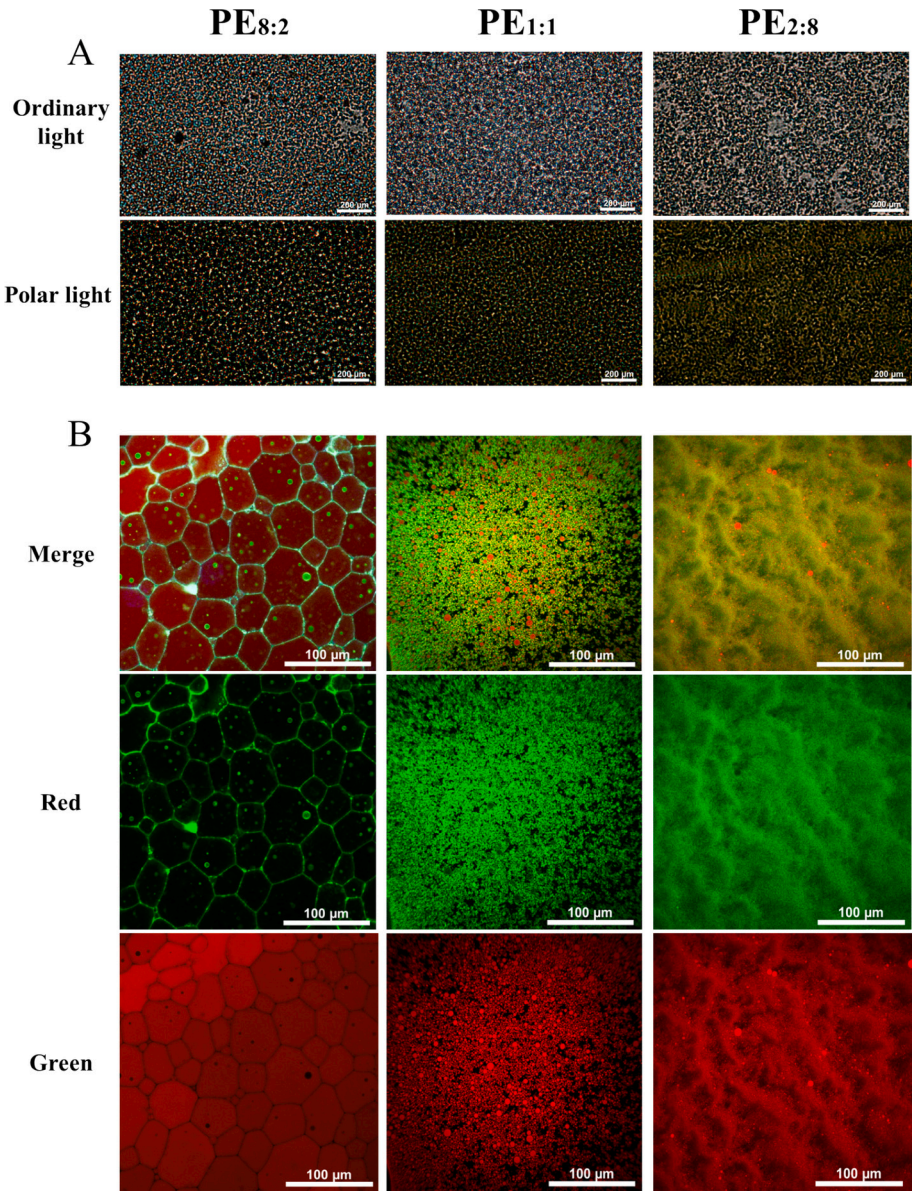

Fig. 4. Microstructural observations of CAF-based PEs ($PE_{8:2}$, $PE_{1:1}$, and $PE_{2:8}$): optical observations (A) and CLSM (B). The scale bar is 20 μm and 100 μm.

3.2.5. *Encapsulation and bioavailability*

Based on previous findings on emulsion stabilization at different oil fractions, PEs stabilized by CAF were employed to encapsulate curcumin. As shown in Fig. 6A, all PEs with varying internal phase ratios exhibited high EE values ranging from 94.59 % to 98.27 %, demonstrating their effective curcumin encapsulation capability. This is attributed to the formation of a dense cross-linked emulsion network, which acts as a barrier to effectively reduce bioactive leakage (Zhao, Wu, et al., 2024). Additionally, to further assess the potential applications of PEs stabilized by CAF, their bioavailability was evaluated, as shown in Fig. 6B. Higher bioavailability was observed in PEs with lower internal phase ratios, likely due to reduced emulsion viscosity that facilitates the free movement of bioactives throughout the system. Furthermore, the formation of smaller droplets in these PEs increased the contact area between enzymes and bioactives (Zhao et al., 2024), as supported by the results in section 3.2.1. Collectively, these findings suggest that PEs stabilized by CAF are promising delivery carriers for enhancing the bioaccessibility of bioactive compounds.

3.2.6. *In vitro digestion evaluation*

To further evaluate the applicability of CAF-based PEs, the digestion behavior at different stages was assessed using an in vitro digestion model, as shown in Fig. 6. During the intestinal digestion phase, the FFA release profiles (Fig. 6C) of all PEs decreased over time. Despite the higher system viscosity and denser emulsion network in high internal phase PEs, $PE_{8:2}$ exhibited the highest FFA release, likely due to increased contact between the larger lipid core and lipase. Similar findings were reported in a previous study (Li, Cao, et al., 2025). Furthermore, **Fig. 6D** and **E** present the average droplet size and zeta potential of PEs at various digestion stages. $PE_{8:2}$ showed the largest droplet size in simulated gastric fluid (SGF), indicating a higher degree of coalescence caused by its inherently larger particle size combined with the low pH and high ionic strength during the gastric phase. For all samples, droplet size decreased during digestion, likely due to the action of bile salts and pancrelipase in the digestive medium. This trend aligns with observations from another study (Yang, Song, Chen, Jiang, et al., 2025). These results demonstrate that CAF-based PEs possess excellent sustained-release properties, thereby improving the delivery efficiency of bioactive compounds. These findings provide valuable insights for the

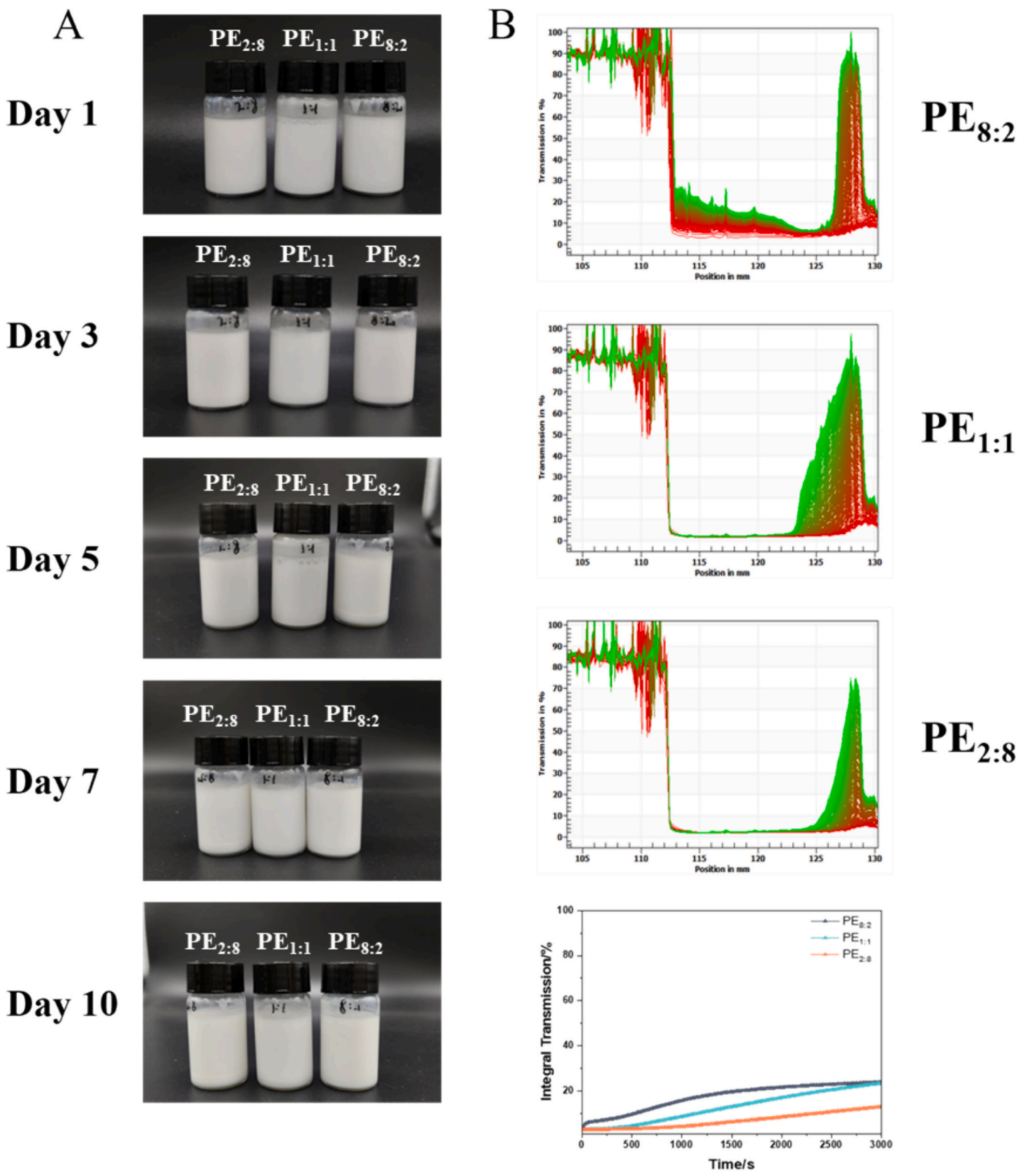

Fig. 5. Stability of CAF-based PEs ($PE_{8:2}$, $PE_{1:1}$, and $PE_{2:8}$): Visual changes over 10 days of storage at 25 °C (A), physical stability (B).

design of delivery systems for bioactive compounds in biomedical applications.

CAF-based PEs exhibit excellent loading and delivery performance for lipophilic bioactive compounds during in vitro digestion studies. These properties arise from the unique structural composition of CAF, featuring a highly hydrophobic core and a hydrophilic protein shell. This structure provides high flexibility and interfacial wettability, facilitating adsorption and reorganization of particle molecules at the oil–water interface during emulsification. Compared with other plant-derived amyloid PEs, CAF-based PEs form a denser network and exhibit superior physical stability. Moreover, their stability under acidic pH conditions contributes to enhanced resistance during gastric digestion.

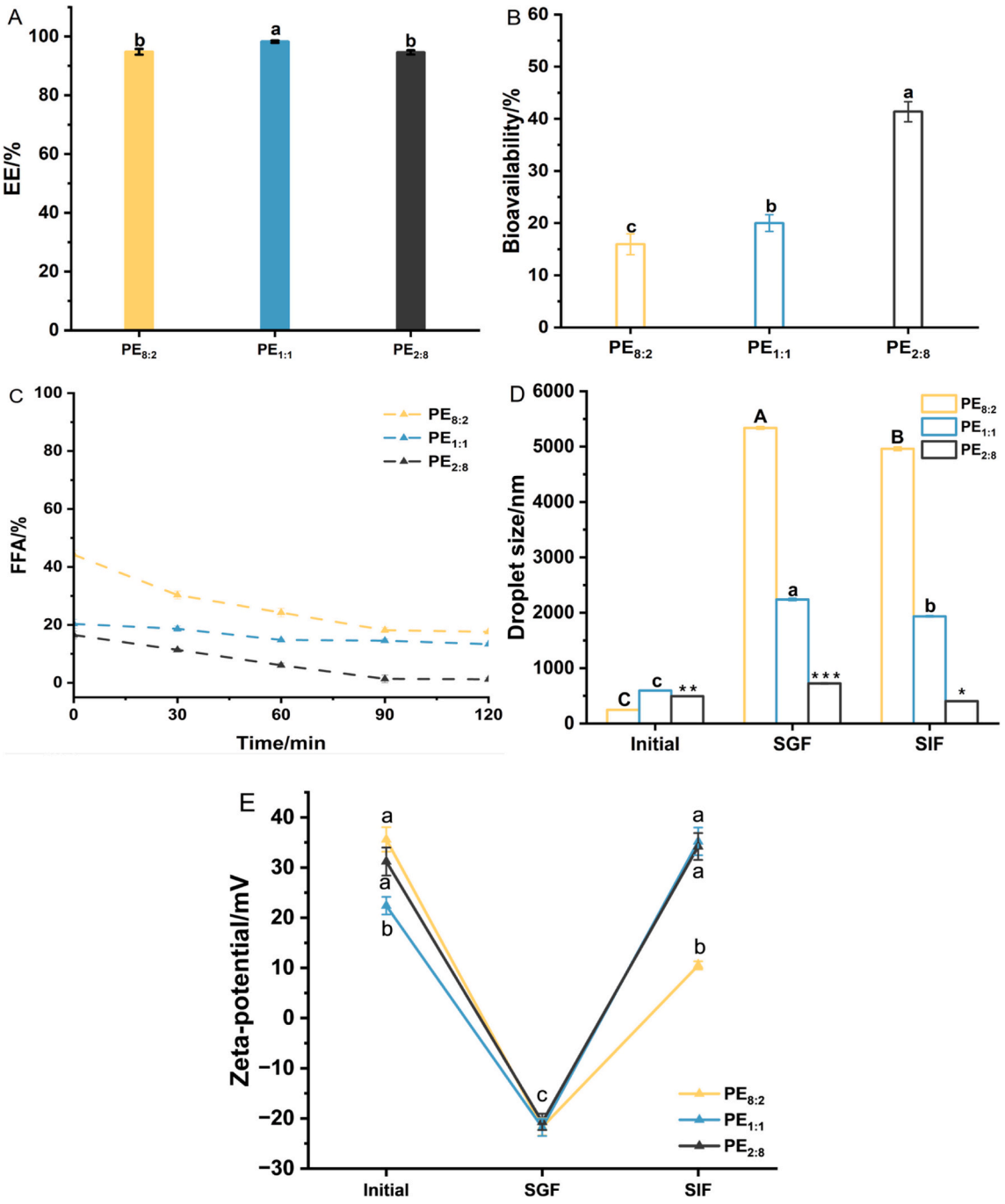

Fig. 6. Encapsulation (A) and bioavailability (B) of CAF-based PEs ($PE_{8:2}$, $PE_{1:1}$, and $PE_{2:8}$). In vitro digestion behavior of CAF-based PEs: FFA (C), droplet size (D), and zeta-potential (E). $^{a\text{-}c,\ A\text{-}C}$ Different letters show significant differences between the samples ($P < 0.05$).

Consequently, CAF-based PEs show strong potential for the effective delivery and sustained release of bioactive compounds.

4. Conclusion

In summary, we firstly developed protein amyloid-like fibrils from coconut protein using acid-heat induction. Our study revealed the effects of varying internal phase ratios on PEs stabilized by CAF. Acid-heat induction produced flexible CAF characterized by an increased random coil shell surrounding an ordered core. Notably, CAF exhibited a positive charge at low pH, facilitating interactions with negatively charged biomacromolecules. The internal phase variations influenced multiple PE properties, including droplet size, zeta potential, rheological behavior, encapsulation efficiency, and physical stability. Importantly, a "blanket-like" cross-linked emulsion network formed via the intertwined connections of CAF, which enhanced emulsion stability and bioactive encapsulation capacity. PEs demonstrated tunable encapsulation efficiency, bioavailability, and digestion profiles depending on the internal phase ratio. This work advances understanding of the assembly and interfacial behavior of plant protein-based amyloid-like fibrils and offers new insights for applications in industries such as amyloid aerogels and innovative delivery systems.

CRediT authorship contribution statement

Yuanyang Song: Writing – original draft, Visualization,

Methodology, Investigation, Formal analysis, Data curation, Conceptualization. **Zhen Yang:** Methodology, Funding acquisition, Formal analysis, Data curation, Conceptualization. **Hui Chen:** Investigation, Formal analysis. **Kaidong Wei:** Formal analysis, Data curation. **Lianzhou Jiang:** Project administration, Methodology, Funding acquisition, Formal analysis. **Zhaoxian Huang:** Writing – review & editing, Supervision, Resources, Project administration, Funding acquisition, Conceptualization.

Declaration of competing interest

The authors declare that they have no known competing financial interests or personal relationships that could have appeared to influence the work reported in this paper.

Acknowledgements

This research was supported by the National Natural Science Foundation of China (32402143), Hainan Province Science and Technology Special Fund (No: ZDYF2025XDNY084 and ZDYF2025XDNY065), Hainan Provincial Natural Science Foundation of China (325QN236), International Science & Technology Cooperation Program of Hainan Province (No: GHYF2025001), and the Graduate Innovation Research Project of Hainan Province (Qhyb2024-27).

Appendix A. Supplementary data

Supplementary data to this article can be found online at https://doi.org/10.1016/j.foodchem.2025.147187.

Data availability

Data will be made available on request.

References

vanden Akker, C. C., Engel, M. F. M., Velikov, K. P., Bonn, M., & Koenderink, G. H. (2011). Morphology and persistence length of amyloid fibrils are correlated to peptide molecular structure. *Journal of the American Chemical Society, 133*(45), 18030–18033. https://doi.org/10.1021/ja206513r

Boostani, S., Riazi, M., Marefati, A., Rayner, M., & Hosseini, S. M. H. (2022). Development and characterization of medium and high internal phase novel multiple Pickering emulsions stabilized by hordein nanoparticles. *Food Chemistry, 372*, Article 131354. https://doi.org/10.1016/j.foodchem.2021.131354

Chen, Y., Li, T., Jiang, L., Huang, Z., Zhang, W., & Luo, Y. (2024). The composition, extraction, functional property, quality, and health benefits of coconut protein: A review. *International Journal of Biological Macromolecules, 280*, Article 135905. https://doi.org/10.1016/j.ijbiomac.2024.135905

Dev, R. K., Yadav, S. N., Shah, P., Magar, N., Ghimire, S., Koirala, M., … Bhattarai, A. (2025). Cetyl pyridinium chloride-amino acid-based ionic liquids: Synthesis, characterization, and physicochemical properties by FT-IR, UV–visible, density, conductivity, viscosity, surface tension, and contact angle studies. *Journal of Ionic Liquids, 5*(1), Article 100158. https://doi.org/10.1016/j.jil.2025.100158

Eisenberg, D. S., & Sawaya, M. R. (2017). Structural studies of amyloid proteins at the molecular level. *Annual Review of Biochemistry, 86*, 69–95. https://doi.org/10.1146/annurev-biochem-061516-045104

Fahim, H., Motamedzadegan, A., Khaligh, N. G., & Farahmandfar, R. (2025). Cellulose nanocrystals (CNC) Pickering emulsions (PEs): Rheological aspects and stability of low-to-medium internal phase. *International Journal of Biological Macromolecules, 312*, Article 144120. https://doi.org/10.1016/j.ijbiomac.2025.144120

Frey, L., Zhou, J., Cereghetti, G., Weber, M. E., Rhyner, D., Pokharna, A., … Mezzenga, R. (2024). A structural rationale for reversible vs irreversible amyloid fibril formation from a single protein. *Nature Communications, 15*(1), 8448. https://doi.org/10.1038/s41467-024-52681-z

Fu, Y., Li, Y., Weng, S., Qi, W., Su, H., & Li, T. (2023). Amyloid protein fibrils show enhanced ice recrystallization inhibition activity when serve as Pickering emulsion stabilizer. *Food Hydrocolloids, 139*, Article 108581. https://doi.org/10.1016/j.foodhyd.2023.108581

Han, T., Qiu, L., Hu, Q., Guo, R., Zhu, Y., Huang, Y., Liu, L., Wang, Y., & Zhu, X. (2026). Amyloid fibrillation of different ratios of 7S/11S soy protein: Comparison of fibril structural characteristics and analysis of the potential for preparing high-internal-phase emulsions. *Food Hydrocolloids, 171*, Article 111781. https://doi.org/10.1016/j.foodhyd.2025.111781

He, C., Xu, Y., Ling, M., Huang, X., & Zhou, Z. (2024). High internal phase emulsions stabilized by walnut protein amyloid-like aggregates and their application in food 3D printing. *Food Hydrocolloids, 147*, Article 109444. https://doi.org/10.1016/j.foodhyd.2023.109444

Hertzler, S. R., Lieblein-Boff, J. C., Weiler, M., & Allgeier, C. (2020). Plant proteins: Assessing their nutritional quality and effects on health and physical function. *In Nutrients, 12*. https://doi.org/10.3390/nu12123704

Isa, L., Jung, J.-M., & Mezzenga, R. (2011). Unravelling adsorption and alignment of amyloid fibrils at interfaces by probe particle tracking. *Soft Matter, 7*(18), 8127–8134. https://doi.org/10.1039/C1SM05602F

Kuzhithariel Remanan, M., & Zhu, F. (2023). Encapsulation of ferulic acid in high internal phase Pickering emulsions stabilized using nonenyl succinic anhydride (NSA) and octenyl succinic anhydride (OSA) modified quinoa and maize starch nanoparticles. *Food Chemistry, 429*, Article 136748. https://doi.org/10.1016/j.foodchem.2023.136748

Li, H., Cao, Y., Wang, L., Wang, F., Xiong, L., Shen, X., & Song, H. (2025). Pickering high internal phase emulsions stabilized by soy protein isolate/κ-carrageenan complex for enhanced stability, bioavailability, and absorption mechanisms of nobiletin. *Carbohydrate Polymers, 351*, Article 123117. https://doi.org/10.1016/j.carbpol.2024.123117

Li, S., Liu, X., Fang, Y., & Cao, Y. (2025). Efficient and source-independent preparation of amyloid fibrils from almond protein isolates and concentrates. *Food Hydrocolloids, 166*, Article 111281. https://doi.org/10.1016/j.foodhyd.2025.111281

Li, T., & Wang, L. (2023). Improved curcumin bioaccessibility in Pickering emulsion fabricated by rice glutelin fibrils. *Food Bioscience, 55*, Article 102988. https://doi.org/10.1016/j.fbio.2023.102988

Li, T., Zhou, J., Peydayesh, M., Yao, Y., Bagnani, M., Kutzli, I., Chen, Z., Wang, L., & Mezzenga, R. (2023). Plant protein amyloid fibrils for multifunctional sustainable materials. *Advanced Sustainable Systems, 7*(4), Article 2200414. https://doi.org/10.1002/adsu.202200414

Liang, Y., Zhang, P., Liu, M., Liu, H., He, B., Zhu, Y., & Wang, J. (2025). Plant-based protein amyloid fibrils: Origins, formation, extraction, applications, and safety. *Food Chemistry, 469*, Article 142559. https://doi.org/10.1016/j.foodchem.2024.142559

Liu, Z.-W., Tang, P.-P., Liu, C., Tan, Y.-C., Liu, T.-L., Cheng, J.-H., … Liu, X.-B. (2025). Promoting ovalbumin amyloid fibrils formation by cold plasma treatment and improving its emulsifying properties. *Food Hydrocolloids, 158*, Article 110531. https://doi.org/10.1016/j.foodhyd.2024.110531

Meng, Y., Wei, Z., & Xue, C. (2022). Protein fibrils from different food sources: A review of fibrillation conditions, properties, applications and research trends. *Trends in Food Science & Technology, 121*, 59–75. https://doi.org/10.1016/j.tifs.2022.01.031

Pang, L., Liu, M., Gao, Y., Chen, C., Zhao, Q., Yang, X., Zhang, W., & Jiang, Y. (2025). Induction of beta-lactoglobulin amyloid fibril formation by acid heating to reduce allergenicity and improve functional properties: Insights from structural changes and protein hydrolysis. *Food Hydrocolloids, 169*, Article 111592. https://doi.org/10.1016/j.foodhyd.2025.111592

Papageorgiou, S. N. (2022). On correlation coefficients and their interpretation. *Journal of Orthodontics, 49*(3), 359–361. https://doi.org/10.1177/14653125221076142

Punzalan, J. M., Hartono, P., Fraser-Miller, S. J., Leong, S. Y., Sutton, K., Moggre, G.-J., … Oey, I. (2025). MicroNIR spectroscopy with chemometric analysis provides rapid protein content evaluation and prediction of semi-refined flaxseed protein extract produced via pulsed electric field (PEF)-assisted extraction. *Food Chemistry, 473*, Article 143062. https://doi.org/10.1016/j.foodchem.2025.143062

Restolho, J., Mata, J. L., & Saramago, B. (2009). On the interfacial behavior of ionic liquids: Surface tensions and contact angles. *Journal of Colloid and Interface Science, 340*(1), 82–86. https://doi.org/10.1016/j.jcis.2009.08.013

Sakuno, M. M., Matsumoto, S., Kawai, S., Taihei, K., & Matsumura, Y. (2008). Adsorption and structural change of β-lactoglobulin at the diacylglycerol− water interface. *Langmuir, 24*(20), 11483–11488. https://doi.org/10.1021/la8018277

Thaiphanit, S., & Anprung, P. (2016). Physicochemical and emulsion properties of edible protein concentrate from coconut (Cocos nucifera L.) processing by-products and the influence of heat treatment. *Food Hydrocolloids, 52*, 756–765. https://doi.org/10.1016/j.foodhyd.2015.08.017

Tran, E., Mapile, A. N., & Richmond, G. L. (2021). Peeling back the layers: Investigating the effects of polyelectrolyte layering on surface structure and stability of oil-in-water nanoemulsions. *Journal of Colloid and Interface Science, 599*, 706–716. https://doi.org/10.1016/j.jcis.2021.04.115

Wang, Z., Liu, X., Li, S., Li, S., Fang, Y., & Cao, Y. (2025). Formation and morphology of flaxseed protein isolate amyloid fibrils as governed by NaCl concentration. *Food Hydrocolloids, 166*, Article 111300. https://doi.org/10.1016/j.foodhyd.2025.111300

Winuprasith, T., & Suphantharika, M. (2015). Properties and stability of oil-in-water emulsions stabilized by microfibrillated cellulose from mangosteen rind. *Food Hydrocolloids, 43*, 690–699. https://doi.org/10.1016/j.foodhyd.2014.07.027

Wu, H., Nian, Y., Liu, Y., Zhang, Y., & Hu, B. (2022). Formation of pea protein amyloid fibrils to stabilize high internal phase emulsions for encapsulation of lutein. *Journal of Functional Foods, 94*, Article 105110. https://doi.org/10.1016/j.foodhyd.2014.07.027

Xiao, J., Qi, X., Qian, Y., Cheng, Y., Gong, J., Shen, M., Shen, L., & Xie, J. (2025). Formation, construction, and functional properties of amyloid fibrils derived from chickpea protein isolate. *Food Research International, 221*, Article 117308. https://doi.org/10.1016/j.foodres.2025.117308

Xu, D., Zhou, J., Soon, W. L., Kutzli, I., Molière, A., Diedrich, S., … Mezzenga, R. (2023). Food amyloid fibrils are safe nutrition ingredients based on in-vitro and in-vivo assessment. *Nature Communications, 14*(1), 6806. https://doi.org/10.1038/s41467-023-42486-x

Xu, Q., Cheng, C., Li, Q., Zhu, G., Wei, Y., & Liu, K. (2025a). Comparison of formation and structural characteristics of amyloid fibrils of peanut protein isolate after

hydration treatment at different pH. *Food Hydrocolloids, 159*, Article 110599. https://doi.org/10.1016/j.foodhyd.2024.110599

Xu, Q., Cheng, C., Li, Q., Zhu, G., Wei, Y., & Liu, K. (2025b). Concentration-regulated fibrillation of peanut protein: Formation, structural characteristics, and emulsifying properties. *Food Hydrocolloids, 167*, Article 111421. https://doi.org/10.1016/j.foodhyd.2025.111421

Xu, Q., Ma, Y., Sun, Y., Li, D., Zhang, X., & Liu, C. (2023). Protein amyloid aggregate: Structure and function. *Aggregate, 4*(4), Article e333. https://doi.org/10.1002/agt2.333

Yang, Z., Song, Y., Chen, L., Jiang, L., Huang, Z., & Wang, L. (2025). High internal phase Pickering emulsions stabilized by soybean glycinin-debranched starch flexible particles: Characterization, rapid formation and slow digestion mechanism. *Food Chemistry, 482*, Article 144184. https://doi.org/10.1016/j.foodchem.2025.144184

Yang, Z., Song, Y., Chen, L., Wang, Z., Wang, L., Guo, Z., Jiang, L., Huang, Z., & Tian, Y. (2025). Soybean β-conglycinin-debranched starch flexible nano-conjugates: Focus on formation mechanism and physicochemical characteristics. *Food Chemistry, 479*, Article 143795. https://doi.org/10.1016/j.foodchem.2025.143795

Yang, Z., Song, Y., Chen, L., Zhang, W., Xie, D., Jiang, L., Huang, Z., & Li, D. (2025). Insight into the structural, interfacial and functional properties of soybean 11S globulin-debranched starch conjugates through alkaline Maillard reaction. *Carbohydrate Polymers, 350*, Article 123054. https://doi.org/10.1016/j.carbpol.2024.123054

Yang, Z., Zeng, C., Chen, L., Tian, T., Wang, Z., Wang, H., Zhang, W., Jiang, L., Huang, Z., & Li, D. (2025). Effects of monosaccharides glycation on structural characteristics and functional properties of coconut protein isolate based on molecular docking. *Food Hydrocolloids, 160*, Article 110868. https://doi.org/10.1016/j.foodhyd.2024.110868

Yue, J., Yao, X., Gou, Q., Li, D., Liu, N., Yang, D., Gao, Z., Midgley, A., Katsuyoshi, N., & Zhao, M. (2022). Recent advances of interfacial and rheological property based techno-functionality of food protein amyloid fibrils. *Food Hydrocolloids, 132*, Article 107827. https://doi.org/10.1016/j.foodhyd.2022.107827

Zhang, H., Wu, Z., Wu, J., Hua, Q., Liang, Y., & Renneckar, S. (2025). High internal phase Pickering emulsions stabilized by surface-modified dialdehyde xylan nanoparticles. *Carbohydrate Polymers, 354*, Article 123324. https://doi.org/10.1016/j.carbpol.2025.123324

Zhao, M., Wu, X., Tan, H., & Wu, W. (2024). Protein oxidation affected the encapsulation properties of rice bran protein fibril-high internal phase Pickering emulsions: Enhanced stability and bioaccessibility of β-carotene. *Food Research International, 192*, Article 114779. https://doi.org/10.1016/j.foodres.2024.114779

Zhao, Y., Liang, Y., Wang, X., Zu, X., & Wang, H. (2024). Utilization of peanut protein isolate amyloid-like fibers as stabilizers for high internal phase Pickering emulsions. *Industrial Crops and Products, 213*, Article 118414. https://doi.org/10.1016/j.indcrop.2024.118414

Zhou, L., Ali, I., Goh, B. H., Fu, J. Y., Manickam, S., Tang, S. Y., & Shen, Q. (2025). Enhancing meat emulsion gels with soy protein fibril and red palm oil Pickering emulsions: The role of emulsification techniques in chicken fat substitution. *LWT, 216*, Article 117348. https://doi.org/10.1016/j.lwt.2025.117348

Zhu, Q., Chen, W., Wang, L., Chen, W., Zhang, M., Zhong, Q., Pei, J., & Chen, H. (2024). Development of high internal phase emulsions using coconut protein isolates modified by pulsed light: Relationship of interfacial behavior and emulsifying stability. *Food Hydrocolloids, 148*, Article 109495. https://doi.org/10.1016/j.foodhyd.2023.109495

Zhu, Q., Qiu, Y., Zhang, L., Lu, W., Pan, Y., Liu, X., Li, Z., & Yang, H. (2024). Encapsulation of lycopene in Pickering emulsion stabilized by complexes of whey protein isolate fibrils and sodium alginate: Physicochemical property, structural characterization and in vitro digestion property. *Food Research International, 191*, Article 114675. https://doi.org/10.1016/j.foodres.2024.114675